

Two-dimensional transition metal halide PdX_2 (X = F, Cl, Br, I): A promising candidate of bipolar magnetic semiconductors

Miao-Miao Chen(陈苗苗), Sheng-Shi Li(李胜世), Wei-Xiao Ji(纪维霄), and Chang-Wen Zhang(张昌文)
Citation: Chin. Phys. B, 2023, 32 (**12**): 127103. DOI: 10.1088/1674-1056/ad04c3
Journal homepage: http://cpb.iphy.ac.cn; http://iopscience.iop.org/cpb

What follows is a list of articles you may be interested in

Design of sign-reversible Berry phase effect in 2D magneto-valley material

Yue-Tong Han(韩曰通), Yu-Xian Yang(杨宇贤), Ping Li(李萍), and Chang-Wen Zhang(张昌文)
Chin. Phys. B, 2023, 32 (**9**): 097101. DOI: 10.1088/1674-1056/acd920

Highly anisotropic Dirac fermion and spin transportproperties in Cu-graphane

Chao Wu(吴超), Lichuan Zhang(张礼川), Lin Xia(夏霖), Dong Hao(郝东), Shiqi Li(李仕琪), Lizhi Zhang(张礼智), Yuee Xie(谢月娥), and Yuanping Chen(陈元平)
Chin. Phys. B, 2023, 32 (**8**): 087104. DOI: 10.1088/1674-1056/accff1

Modulation of CO adsorption on 4,12,2-graphyne by Fe atom doping and applied electric field

Yu Dong(董煜), Zhi-Gang Shao(邵志刚), Cang-Long Wang(王苍龙), and Lei Yang(杨磊)
Chin. Phys. B, 2023, 32 (**8**): 087101. DOI: 10.1088/1674-1056/acc935

High-temperature ferromagnetism and strong π-conjugation feature in two-dimensional manganese tetranitride

Ming Yan(闫明), Zhi-Yuan Xie(谢志远), and Miao Gao(高淼)
Chin. Phys. B, 2023, 32 (**3**): 037104. DOI: 10.1088/1674-1056/acae7b

Magnetic and electronic properties of two-dimensional metal-organic frameworks $TM_3(C_2NH)_{12}$

Zhen Feng(冯振), Yi Li(李依), Yaqiang Ma(马亚强), Yipeng An(安义鹏), and Xianqi Dai(戴宪起)
Chin. Phys. B, 2021, 30 (**9**): 097102. DOI: 10.1088/1674-1056/ac0cdb

---

Two-dimensional transition metal halide PdX_2 (X = F, Cl, Br, I): A promising candidate of bipolar magnetic semiconductors

Miao-Miao Chen(陈苗苗), Sheng-Shi Li(李胜世), Wei-Xiao Ji(纪维霄), and Chang-Wen Zhang(张昌文)†

School of Physics and Technology, Institute of Spintronics, University of Jinan, Jinan 250022, *China*

(Received 14 July 2023; revised manuscript received 6 October 2023; accepted manuscript online 19 October 2023)

Two-dimensional (2D) nanomaterials with bipolar magnetism show great promise in spintronic applications. Manipulating carriers' spin-polarized orientation in bipolar magnetic semiconductor (BMS) requires a gate voltage, but that is volatile. Recently, a new method has been proposed to solve the problem of volatility by introducing a ferroelectric gate with proper band alignment. In this paper, we predict that the PdX_2 (X = F, Cl, Br, I) monolayers are 2D ferromagnetic BMS with dynamic stability, thermal stability, and mechanical stability by first-principles calculations. The critical temperatures are higher than the boiling point of liquid nitrogen and the BMS characteristics are robust against external strains and electric fields for $PdCl_2$ and $PdBr_2$. Then, we manipulate the spin-polarization of $PdCl_2$ and $PdBr_2$ by introducing a ferroelectric gate to enable magnetic half-metal/semiconductor switching and spin-up/down polarization switching control. Two kinds of spin devices (multiferroic memory and spin filter) have been proposed to realize the spin-polarized directions of electrons. These results demonstrate that $PdCl_2$ and $PdBr_2$ with BMS characters can be widely used as a general material structure for spintronic devices.

Keywords: PdX_2 (X = F, Cl, Br, I), bipolar magnetic semiconductors, first-principles calculations

PACS: 71.38.Mx, 75.50.Pp, 73.20.At **DOI:** 10.1088/1674-1056/ad04c3

1. Introduction

Recently, the development of high-performance two-dimensional (2D) spintronic nanodevices has attracted widespread attention, with the current mainstream trend of miniaturization of electronic information devices.[1–8] The generation of 100% spin-polarized currents and manipulation of carriers' spin polarization at the Fermi level (E_F) are two key challenges for the development of high-performance 2D spintronic nanodevices. Half-metals (HMs),[9] with one metallic spin channel and another semiconducting channel, are highly desired because they provide 100% spin-polarized currents, but they have a fixed spin direction. Conventionally, the directions of spin polarization in materials can be manipulated by a magnetic field, whereas it is hard to be complicated in operation and useful only for certain materials and has an adverse impact on adjacent device parts.[10–18] The proposal of bipolar magnetic semiconductor (BMS)[19] material solves the problems, which allows us to achieve HM with different conductive spin channels by applying a gate voltage. This depends on their unique electronic structure: the valence band (VB) and the conduction band (CB) have opposite spin polarizations near the E_F.[20,21] However, the method requires persistent electrical control which is volatile and achieved by applying a gate voltage.[19,20,22] So far, although there are many theoretically predicted BMS materials,[23–27] the experimental realization of BMS[28] is still lacking, as the large leakage current hinders its application in memory storage devices.[29] Recently, Li and Deng *et al.*[30] proposed a new method to manipulate both spin-polarized orientations in BMS materials by the introduction of a ferroelectric (FE) gate with proper band alignment. Compared with traditional electrical control approaches, the method can overcome volatility, which is more energy-efficiency. Thus, it is emergent to search for and design experimentally reachable 2D BMS.

In this work, we first study the geometric, electronic, and magnetic properties of PdX_2 (X = F, Cl, Br, I) monolayers. It is found that $PdCl_2$, $PdBr_2$, and PdI_2 monolayers are outstanding candidates for spintronic materials and are possible to construct different spin-polarization transport channels in a single material by carrier doping. Hence, they are highly likely to become a material for spin field effect transistors (FET). Then we explore the robustness of $PdCl_2$, $PdBr_2$, and PdI_2 under external strains and strong electric fields and find that only the BMS properties of $PdCl_2$ and $PdBr_2$ are robust against external strains and strong electric fields. Furthermore, we introduce Ga_2S_3 and Ga_2Se_3 with different ferroelectric polarization to realize the nonvolatile spin polarization regulation of $PdCl_2$ and $PdBr_2$. Finally, based on this, we design a multiferroic memory device and a spin filter device. Our research provides theoretical support for the experimental implementation of BMS.

2. Computational details

All of our density theory functional (DFT) calculations use the projection-enhanced wave (PAW) method,[31] which is implemented in the Vienna *ab initio* simulation pack-

†Corresponding author. E-mail: ss_zhangchw@ujn.edu.cn

© 2023 Chinese Physical Society and IOP Publishing Ltd

age (VASP).[32,33] The paper uses Perdew–Burke–Ernzerhof (PBE) functional[34] to describe the correlation and exchange interactions of PdX_2. The strong correlation effects for the Pd-4d electrons use the PBE+U method[35] and the Hubbard U parameter is 3.5 eV. Then we employ the Heyd–Scuseria–Ernzerhof hybrid functional method (HSE06)[36] to obtain the accurate band structures. The cutoff energy is set to 400 eV. The Brillouin zone is sampled by using a $9\times9\times1$ k-mesh. To avoid interactions between adjacent layers, a vacuum space of 20 Å is applied along the z-axis [001] direction. The convergence criteria for the energy and residual force on each atom are 1×10^{-8} eV and 0.001 eV/Å. The phonon calculations are carried out by using density-functional perturbation theory as implemented in the PHONOPY code[37] combined with VASP. The *ab initio* molecular dynamics (AIMD)[38] simulation is performed with a $4\times4\times1$ supercell at 100 K temperature. The van der Waals (vdW)[39,40] is employed and a vacuum space greater than 30 Å or 40 Å is applied for the bilayer or three-layer heterostructures. The VASPKIT code is used to process some of the VASP data.[41] The Curie temperature is estimated by using the Monte Carlo simulation package MCSOLVER code[42] based on the Wolff algorithm.

3. Result and discussion

The PdX_2 (X = F, Cl, Br, I) monolayers share two possible phases, which are similar to classical 2D material $PbBr_2$ and PbI_2,[43–52] namely, T (Fig. 1(a)) and H (Fig. 1(b)) phases. The Pd atomic layer is sandwiched by the upper and lower F/Cl/Br/I atomic layers, with atoms in each layer forming a 2D hexagonal lattice. In order to study more optimal configurations in terms of energy, the energy difference is calculated between the T and H configurations ($\Delta E_{\mathrm{T-H}}$). The lattice constant (a) and the $\Delta E_{\mathrm{T-H}}$ of PdX_2 monolayers are shown in Table S1. The optimized lattice constants (T/H) of PdF_2, $PdCl_2$, $PdBr_2$, and PdI_2 monolayers are 3.30/3.38 Å, 3.70/3.54 Å, 3.87/3.72 Å, and 4.11/3.97 Å, respectively. With the increase of the X atomic order, the lattice constant is increasing, meeting the positive correlation between lattice constants and atomic radius. All $\Delta E_{\mathrm{T-H}}$ of the PdX_2 monolayers are negative, which indicates that the PdX_2 monolayers tend to form in the 1T configuration. Our works only consider the PdX_2 (X = F, Cl, Br, I) monolayers that are formed in the T phases.

Before confirming the magnetic and electronic properties of PdX_2, we explore their stabilities (including dynamic stability, thermal stability, and mechanical stability). The formation energy E_{form} is evaluated as

$$E_{\mathrm{form}} = \left(\mu_{\mathrm{Pd}} + \mu_{X_2} - E_{PdX_2}\right)/3, \tag{1}$$

where μ_{Pd} is the chemical potential of the Pd bulk and μ_{X_2} is the energy of the X molecule. The calculated formation energies are listed in Table S1. The positive values demonstrate that the iodination is an exothermal process, suggesting the feasibility of the experimental synthesis of these materials. The phonon dispersion curves are calculated with a $5\times5\times1$ supercell using the PHONOPY package through the density functional perturbation theory.[53] As indicated in Fig. S1, all the phonon frequencies of PdX_2 monolayers are positive in the first Brillouin zone, which proves the excellent dynamic stabilities of PdX_2 monolayers. To examine the thermal stabilities of the PdX_2 monolayer, the AIMD simulations are evaluated in the canonical ensemble on a $5\times5\times1$ supercell. Four images of Fig. S2 indicate the total energies of PdF_2, $PdCl_2$, $PdBr_2$, and PdI_2 monolayers, respectively. It can be seen that total energies have slightly fluctuated around the equilibrium value during the simulations and there is no destruction for the materials after 10000 fs, indicating the thermal stabilities of the PdF_2, $PdCl_2$, $PdBr_2$, and PdI_2 monolayers under 100 K. Because of the $p\bar{3}m1$ space group, by using Voigt symbols, the elastic tensor of PdX_2 can be reduced to[54]

$$\boldsymbol{C} = \begin{pmatrix} C_{11} & C_{12} & 0 \\ C_{12} & C_{11} & 0 \\ 0 & 0 & \frac{C_{11}-C_{12}}{2} \end{pmatrix}. \tag{2}$$

The independent C_{11}, C_{12}, and $C_{11}-C_{12}$ of PdX_2 are shown in Table S1. It can be found that the PdX_2 (X = F, Cl, Br, I) monolayers satisfy the Born–Huang criterion for two-dimensional hexagonal planes ($C_{11}>0$ and $C_{11}-C_{12}>0$),[56] which means that the PdX_2 monolayers are mechanically stable.

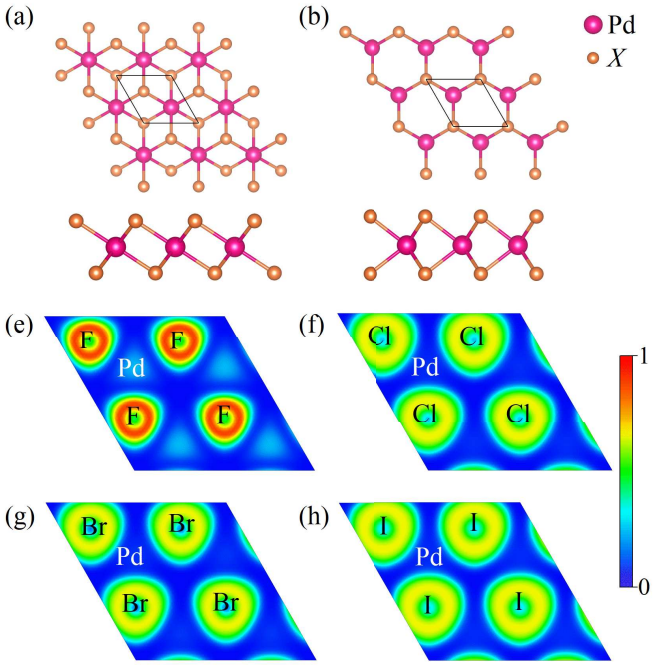


Fig. 1. The crystal structures of PdX_2 (X = F, Cl, Br, I) monolayers in T (a) and H (b) phases: top and side views. The electron localization functions for PdF_2 (c), $PdCl_2$ (d), $PdBr_2$ (e), and PdI_2 (f). Pd, F, Cl, Br, and I atoms are annotated accordingly.

To determine the magnetic ground states of the PdX_2 monolayers, the total energy differences (Table S1), including the ferromagnetic (FM) and three antiferromagnetic (AFM) states (Fig. S3(a)), are compared by using the supercell. Table S1 shows that the calculated total energies of the AFM are higher than that of the FM state for PdF_2, $PdCl_2$, $PdBr_2$, and PdI_2 monolayers, which indicates the magnetic ground states of the PdX_2 monolayers are FM state. While $PbBr_2$ is an inherently nonmagnetic semiconductor,[52] this is due to the different electronic configurations of the Pd and Pb atoms. We track the physical originations of FM coupling in PdX_2 monolayers by the super-exchange interactions, which can be comprehended by the Pd–X–Pd bond angle θ (Table 1). The values of θ are 97.88°, 93.49°, 92.64°, and 92.56°for PdF_2, $PdCl_2$, $PdBr_2$, and PdI_2, respectively, closed to 90°. According to the Goodenough–Kanamori–Anderson (GKA) rules,[55] PdX_2 monolayers possess FM coupling.

The electron localization functions (ELF)[56–58] are plotted to investigate the bonding character of PdF_2, $PdCl_2$, $PdBr_2$, and PdI_2 monolayers in Fig. 1. The (001) section of the ELF confirms that electrons are highly localized around the Pd and F/Cl/Br/I atoms and that electrons are absent between them, indicating the typical ionic character between the Pd–X bonds. Our Bader charge analyses[59] further reveal that the significant electrons respectively transfer 1.2, 0.74, 0.53, and 0.20 electrons from the Pd to F/Cl/Br/I atoms (Table 1), which fall with the electronegativity of F, CI, Br, and I reduced.

Table 1. The Pd–X–Pd bond angle θ and charge transfer number (Δe^-) per unit cell for PdX_2 (X = F, Cl, Br, I) monolayers.

Systems	θ	Δe^-
PdF_2	97.88°	1.20
$PdCl_2$	93.49°	0.74
$PdBr_2$	92.64°	0.53
PdI_2	92.56°	0.20

We used the PBE + U method for the calculations of the electronic structures (Fig. 2). The VBs of the PdF_2, $PdCl_2$, $PdBr_2$, and PdI_2 monolayers possess spin-up polarization when they approach E_F, while their CBs possess spin-down polarization when they approach E_F. The PdF_2 monolayer is a direct bandgap semiconductor with a value of 2.14 eV (Fig. 2(a)). The $PdCl_2$, $PdBr_2$, and PdI_2 monolayers are the indirect bandgap semiconductors, and their band gaps are 1.33 eV, 0.88 eV, and 0.34 eV, respectively (Figs. 2(b)–2(d)). The above results show that the PdF_2, $PdCl_2$, $PdBr_2$, and PdI_2 monolayers are BMS. To confirm the results, the more accurate HSE06 calculations (Figs. S4(a) and S4(b)) further display that although the band gaps increase to 3.56 eV, 2.24 eV, 1.65 eV, and 1.01 eV for PdF_2, $PdCl_2$, $PdBr_2$, and PdI_2, respectively, the VBs and the CBs have opposite spin polarizations near the E_F, indicating that the BMS remains in the four systems.

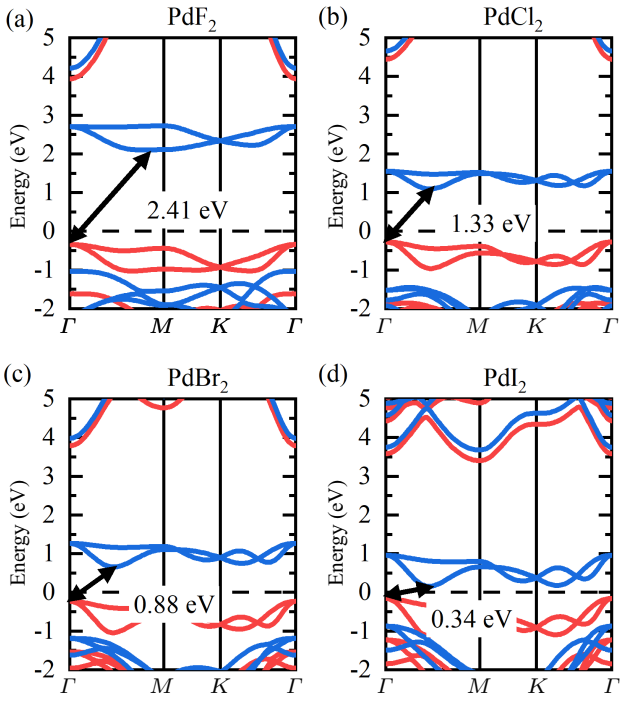


Fig. 2. The electronic band structures based on the PBE+U functional for PdF_2 (a), $PdCl_2$ (b), $PdBr_2$ (c), and PdI_2 (d).

After having demonstrated the bipolar magnetic properties, we now turn to the formation mechanism of BMS for PdX_2 monolayers by crystal field theory. Under the octahedral crystal fields of PdX_2 (Fig. 3(a)), the d orbitals of Pd split into t_{2g} ($d_{xy}/d_{yz}/d_{xz}$) and e_g ($d_{x^2-y^2}/d_{z^2}$) with a splitting gap (Δ_c). According to the electronegativity and nominal valence state Pd^{2+}, the t_{2g} orbitals and the e_g orbitals of the spin-up channel are occupied by six electrons and two electrons, respectively, consistent with the calculated magnetic moment $2\mu_B$. Here, the spin splitting exchange interactions lead the electronic states of the magnetic atom in VBMs and CBMs to belong to different spin channels. It can be attested by their density of states (DOS; Fig. S4(b)). The DOS shows that the spin-exchange splitting (Δ_s) of them are the primary causes of bandgap and the CBM and VBM of PdX_2 are mainly contributed by Pd atoms. The BMSs in PdX_2 are derived from the strength of on-site Coulomb repulsion and the crystal field effect, which are coincident with the report.[60] The d electronic states of the PdX_2 monolayer near the Fermi surface, which usually leads to ferromagnetism, verifying the FM ground state.

The influence of temperature on magnetism is crucial for the practical application of spin electronic devices. Based on the following formulas, the spin Hamiltonian can be described as

$$H = -J\boldsymbol{S}_i\boldsymbol{S}_j - D\left(S_i^Z\right)^2, \tag{3}$$

where J, $\boldsymbol{S}_i$, D, and S_i^Z are the nearest magnetic exchange interaction parameter, the spin vector of each atom, the anisotropy energy parameter, and the Z component of the spin

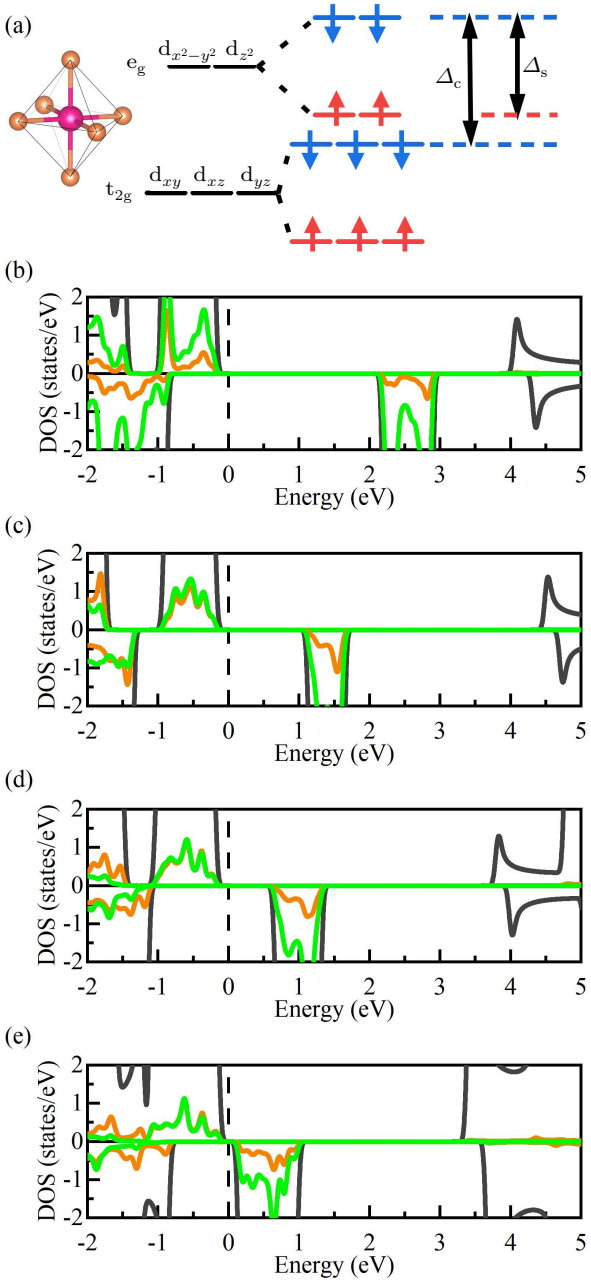


Fig. 3. (a) The schematic diagram of the d-orbital electron occupation of Pd atoms. (b)–(e) The density of states (DOS) for PdF_2, $PdCl_2$, $PdBr_2$ and PdI_2. The gray, orange, and green solid lines represent the total DOS rotated up or down, the DOS contributed by Pd-4d, and the DOS contributed by X-p orbitals, respectively.

vector, respectively. The positive and negative values of J depend on the FM and AFM orders, respectively,

$$E_{\mathrm{FM}} = E_0 - 12J|S|^2 - D|S|^2, \tag{4}$$

$$E_{\mathrm{AFM}} = E_0 + 4J|S|^2 - D|S|^2, \tag{5}$$

where the E_{FM} and E_{AFM} represent the total energy of systems with FM and AFM ordering. The values of J can be estimated as

$$J = \frac{E_{\mathrm{AFM}} - E_{\mathrm{FM}}}{16|S|^2}. \tag{6}$$

The computed J for 2D PdX_2 (X = F, Cl, Br, I) are 0.67 meV, 8.67 meV, 10.30 meV, and 13.10 meV, respectively. Then their magnetic anisotropy energies (MAE) are calculated. The MAE is defined as the energy difference MAE $= E_{001} - E_{100}$ between the out-of-plane (001) and the in-plane (100) magnetization directions by incorporating the SOC effect. The MAE are 61 μeV, 77 μeV, 60 μeV, −982 μeV for the PdF_2, $PdCl_2$, $PdBr_2$, and PdI_2 monolayers, respectively. It indicates that there are the Berezinskii–Kosterlitz–Thouless (BKT)[61] magnetic transition at a critical temperature (T_C) for PdF_2, $PdCl_2$, and $PdBr_2$ monolayers, which can be estimated as $T_C = 0.89J/k_B$. Here k_B is the Boltzmann constant. We get that the T_C for PdF_2, $PdCl_2$, and $PdBr_2$ monolayers are around 7 K, 90 K, and 106 K with their J, above the boiling point of liquid nitrogen (77 K) for $PdCl_2$ and $PdBr_2$ monolayers. Figure S4(b) shows that the PdI_2 monolayer has an estimated Curie temperature of 503 K, notably far above room temperature (300 K). Overall, except for PdF_2, all others are apparently outstanding candidates for spintronic materials. The $PdCl_2$, $PdBr_2$, and PdI_2 monolayers will be studied in the following.

Having evaluated the magnetic properties of $PdCl_2$, $PdBr_2$, and PdI_2 monolayers, we further turn to whether spin polarization can be controlled through electron/hole doping since introducing an FE gate to control the spin polarization of BMS is equivalent to carrier doping, as shown in Fig. S5. We take Fig. S5(a) for example, when 0.1–0.5 electrons are doped, the CBs of $PdCl_2$ are crossed by the Fermi energy level, and the material becomes an HM with the spin-up channel. Doping 0.1–0.5 holes will drive the E_F to transverse with VBs, and become the HM of the spin-down channel. The introduction of a FE gate is expected to realize the control of spin polarization.

In device fabrication, it is likely to introduce strain due to the lattice mismatch between the 2D material and the substrate, and there may be the electric interference from the environment or neighboring electric device. Therefore, we rationalize the robustness of $PdCl_2$, $PdBr_2$, and PdI_2 monolayers under the electric fields and strains. Firstly, the biaxial strains are applied to $PdCl_2$, $PdBr_2$, and PdI_2 monolayers (Fig. S6). Strains are defined as $\varepsilon = (a_1 - a_0)/a_0$, where a_1 and a_0 are lattice constants of PdX_2 with and without deformation, respectively. The negatively and positively valued ε represent compression and tension, respectively. The BMS characteristics are well preserved at $-10\% < \varepsilon < 10\%$ for $PdCl_2$ and $PdBr_2$ (Figs. S7(a) and S7(b)). With 2%–10% compressive strain, the semiconductor PdI_2 firstly changes to HM, then metallic, but that remains unchanged with tensile strain. Secondly, we investigate the robustness of the BMS property to electrical interference from the environment or a neighboring electrical device. Figures S7(a)–S7(c) displays the band structures of $PdCl_2$, $PdBr_2$, and PdI_2 under the electric field of 0.1–0.5 V/Å, respectively. Clearly, under the strong electric field of 0.5 V/Å, the Fermi energy levels of $PdCl_2$ and $PdBr_2$ are

vibrated between the VBM and the CBM. The semiconductor changes to metal for PdI_2 under the electric fields (Fig. S7(c)). Moreover, the calculation of the value of ΔE_{FM-AFM} (Fig. S8) is performed to check the magnetic ground states of $PdCl_2$, $PdBr_2$, and PdI_2 monolayers, and we find that the energetically favorable magnetic configurations are still the FM coupling in the cases of the electric fields and strains. In short, only $PdCl_2$ and $PdBr_2$ monolayers exhibit robustness under the electric fields and strains and are likely to become the experimentally achievable devices. Therefore, we have only conducted research on nonvolatile electric control of spin polarization for $PdCl_2$ and $PdBr_2$ structures below.

We screen Ga_2S_3 and Ga_2Se_3 from the family of 2D FE III2–VI3 materials[62] by comparing the lattice mismatch. The optimized lattice constant of the Ga_2S_3 and Ga_2Se_3 with vdW corrections are 3.70 Å and 3.88 Å, respectively. Subsequently, we construct two multiferroic vdW heterostructures ($PdCl_2/Ga_2S_3$ and $PdBr_2/Ga_2Se_3$), whose lattice mismatch are 0.02% and 0.36%. Three possible stacking patterns are investigated as shown in Fig. 4, denoted as configurations I–III. Our calculations show that configuration-III (Figs. 4(c) and 4(f)) is energetically the most favorable configuration for both upward polarization (P↑) and downward polarization (P↓), this stacking pattern will be researched in the following sections. The binding energy of multiferroic vdW heterostructure is defined as

$$E_b = E_{BMS/FE} - E_{BMS} - E_{FE}, \tag{7}$$

where $E_{BMS/FE}$, E_{BMS} and E_{FE} represent the energies of the BMS/FE heterostructure, BMS layer and the FE layer, respectively. The cohesive energies of $PdCl_2/Ga_2S_3$(P↑), $PdCl_2/Ga_2S_3$(P↓), $PdBr_2/Ga_2Se_3$(P↑), and $PdBr_2/Ga_2Se_3$(P↓) are about −1.89 eV, −1.25 eV, −2.14 eV, and −1.41 eV, respectively, indicating that the heterostructure can be feasible to explore experimentally and stably exist.

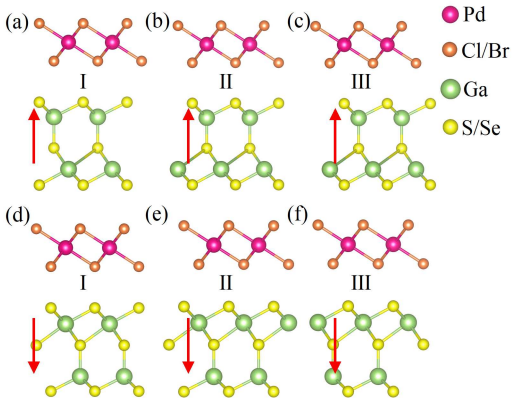


Fig. 4. Three possible stacking modes with upward polarization (a)–(c) and downward polarization (d)–(f) for $PdCl_2/Ga_2S_3$ and $PdBr_2/Ga_2Se_3$ heterostructures.

Then we discuss the density of states (DOS) of the $PdCl_2/Ga_2S_3$ and $PdBr_2/Ga_2Se_3$ heterostructures. Here red and blue symbols denote the contributions from spin-up and spin-down electronic states of $PdCl_2$, $PdBr_2$, Ga_2S_3, and Ga_2Se_3, respectively. Figures 5(a) and 5(c) display that the E_F crosses the minority spin-down bands of the $PdCl_2$ and $PdBr_2$ for $PdCl_2/Ga_2S_3$(P↑) and $PdBr_2/Ga_2Se_3$(P↑), respectively, leading to a half-metal behavior in $PdCl_2$ and $PdBr_2$. Figures 5(b) and 5(d) show that the semiconductor natures of $PdCl_2$ and $PdBr_2$ are retained for $PdCl_2/Ga_2S_3$(P↓) and $PdBr_2/Ga_2Se_3$(P↓), respectively.

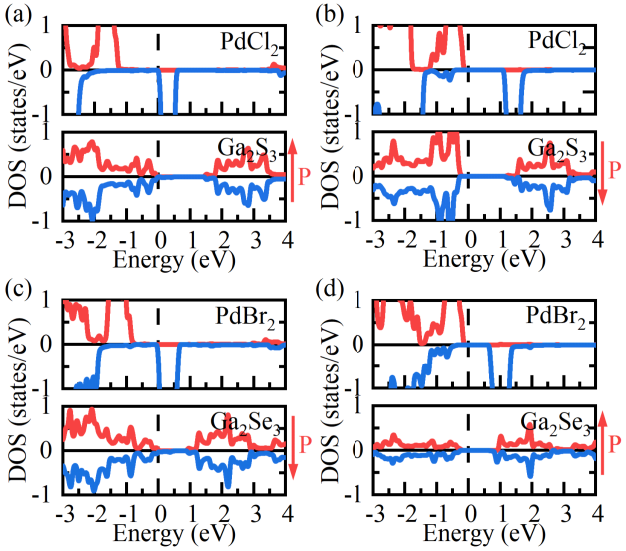


Fig. 5. DOS of $PdCl_2/Ga_2S_3$ and $PdBr_2/Ga_2Se_3$ for P↑ and P↓. The solid red and blue lines represent the DOS contributed by BMS and FE, respectively.

Next, the plane-average potential and the charge density difference of different heterointerfaces are calculated for understanding the mechanism of the electrically controlled semiconductor/half-metal transition. For the P↑, the potential energies of the BMS layer $PdCl_2$ and $PdBr_2$ are lower than that of the FE layer Ga_2S_3 and Ga_2Se_3, respectively (Figs. 6(a) and 6(c)), which can generate that the spin-down CBM of $PdCl_2$ and $PdBr_2$ is lower than the VBM of Ga_2S_3 and Ga_2Se_3, respectively, meaning that there are electrons transfer at the heterostructure interface.

The charge density difference suggests that electron transfer occurs only at the interface between Ga_2Se_3(P↑) and $PdBr_2$ (Fig. S9(c)), while there are almost no electrons accumulating around the interface between Ga_2S_3(P↑) and $PdCl_2$ (Fig. S9(a)). This is consistent with the DOS (Fig. 5(a)) showing that the E_F crosses minority spin-down bands of $PdCl_2$. On the contrary, although the potential energies of the BMS layer $PdCl_2$ and $PdBr_2$ are lower (Figs. 6(b) and 6(d)), the CBMs of Ga_2S_3 and Ga_2Se_3 are still slightly higher than the spin-down VBM of $PdCl_2$ and $PdBr_2$, respectively. This can hinder the spontaneous diffusion of holes for the P↓. The charge density difference suggests that a small number of holes is still insufficient to make the E_F of $PdCl_2$ and $PdBr_2$ cross the spin-up bands (Figs. S9(b) and S9(d)). Hence, the realizations of

the half-metallicity are dependent upon the polarization fields of the FE layer Ga_2S_3 and Ga_2Se_3 and the charge transfer at the interface between the FE and BMS layers for $PdCl_2$ and $PdBr_2$.

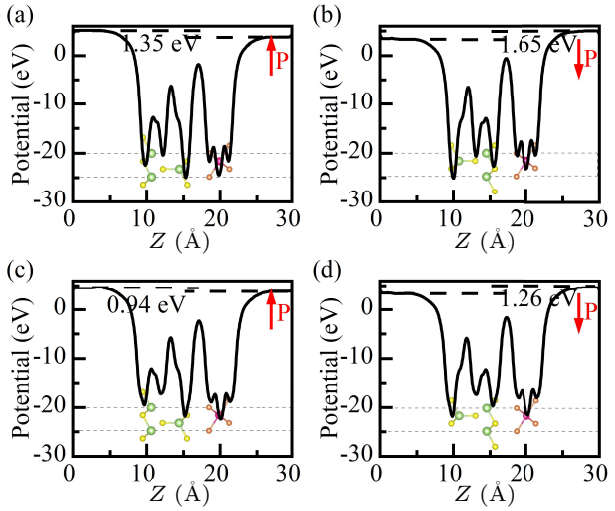


Fig. 6. Plane-averaged potential of $PdCl_2/Ga_2S_3$ and $PdBr_2/Ga_2Se_3$ bilayer heterostructures along the z-direction for P↑ and P↓.

In a word, the generated electric polarizations for Ga_2S_3(P↓) and Ga_2Se_3(P↓) can drive the downward shift of the E_F of $PdCl_2$ and $PdBr_2$, which offers an opportunity to achieve nonvolatile electrical control of spin polarization in $PdCl_2$ and $PdBr_2$ by enhancing polarization field.[63,64] Then we add the Ga_2S_3 and Ga_2Se_3 to the bottom of $PdCl_2/Ga_2S_3$ and $PdBr_2/Ga_2Se_3$ (Figs. 7(a) and 7(b)), respectively. The vdW heterostructures are named $PdCl_2$/bi-Ga_2S_3 and $PdBr_2$/bi-Ga_2Se_3, respectively. Two different polar configurations are taken into account for bi-Ga_2S_3 and bi-Ga_2Se_3, i.e., the polarization directions of FE layers were both pointing upward (P↑↑) or downward (P↓↓).

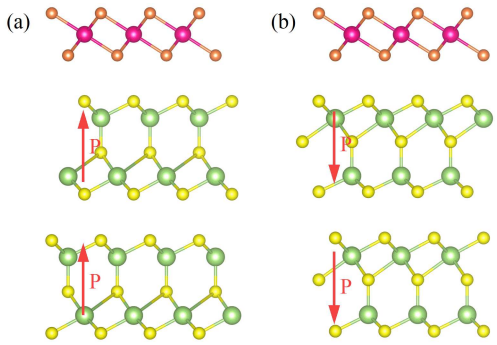


Fig. 7. The vdW heterostructures of $PdCl_2$/bi-Ga_2S_3 and $PdBr_2$/bi-Ga_2Se_3 for P↑↑ and P↓↓.

The binding energies of $PdCl_2$/bi-Ga_2S_3(P↑↑), $PdCl_2$/bi-Ga_2S_3(P↓↓), $PdBr_2$/bi-Ga_2Se_3(P↑↑), and $PdBr_2$/bi-Ga_2Se_3(P↓↓) are −2.71 eV, −2.64 eV, −2.97 eV, and −2.88 eV, respectively, testifying that they are stable. As expected, the DOS of $PdCl_2$/bi-Ga_2S_3 and $PdBr_2$/bi-Ga_2Se_3 trilayer heterostructures (Fig. 8) show that the BMS $PdCl_2$ and $PdBr_2$ become the spin-up (spin-down) HM for P↑↑ (P↓↓), manifested that the nonvolatile spin polarization regulation of $PdCl_2$ and $PdBr_2$ can be achieved by introducing the bilayer FE gates.

After the above discussion, we find that the $PdCl_2/Ga_2S_3$ and $PdBr_2/Ga_2Se_3$ heterostructures possess the capacity to control the HM, and the $PdCl_2$/bi-Ga_2S_3 and $PdBr_2$/bi-Ga_2Se_3 possess the capacity of controlling the spin polarization of BMS.

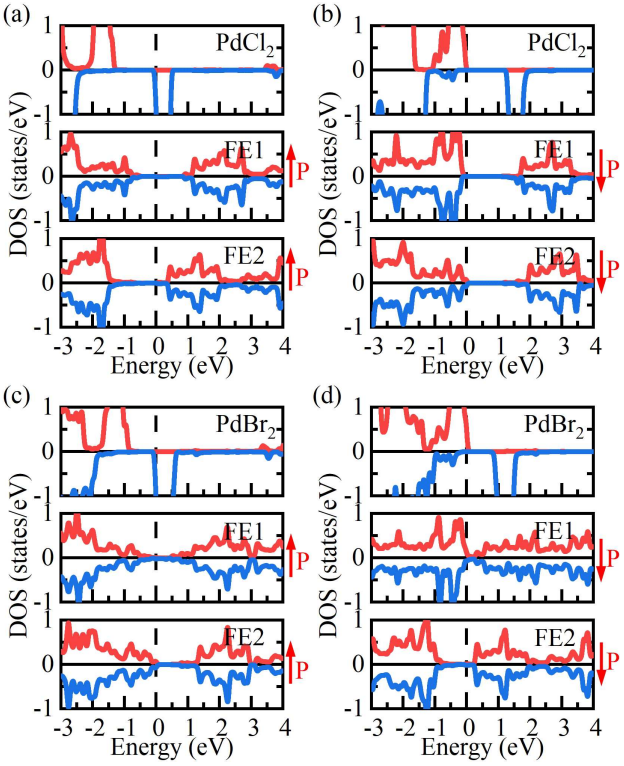


Fig. 8. DOS of $PdCl_2$/bi-Ga_2S_3 or $PdBr_2$/bi-Ga_2Se_3 for P↑ and P↓. The solid red and blue lines represent the DOS contributed by BMS and FE, respectively.

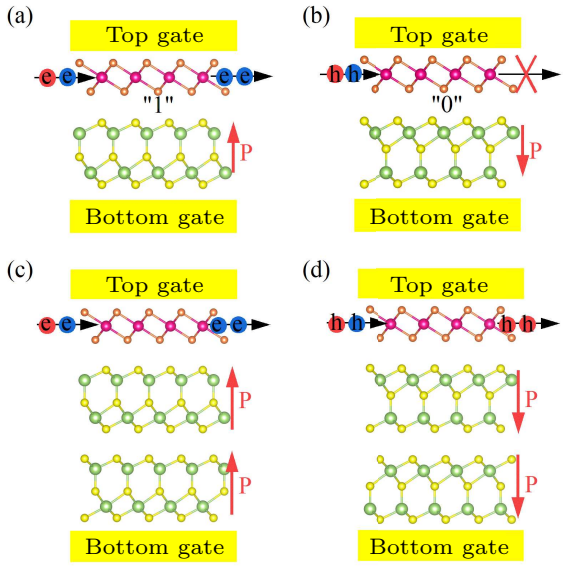


Fig. 9. (a) and (b) The multiferroic memory device. (c) and (d) The spin filter device.

Therefore, the multiferroic memory device (Figs. 9(a) and 9(b)) are designed for the bilayer heterostructures. The P↑ is equivalent to the "1" state (Fig. 9(a)), while the P↓ is equivalent to the "0" state (Fig. 9(b)). In this context, the data reading process is accessible by detecting the electrical signals, and the data reading process is accessible by switching the FE polarized states, thus avoiding the destructive effect caused by detecting the polarized state. Then the spin filter device (Figs. 9(c) and 9(d)) is constructed for the trilayer heterostructures. The electron would travel through the BMS layer, becoming the HM with 100% spin-down polarization at the P↑↑, which is n-type doped. Conversely, the spin-up electrons can pass through the BMS layer at the P↓↓. In short, the manipulation of spin-polarized current can be achieved in this device.

4. Conclusion

In summary, we predict that the PdX_2 (X = F, Cl, Br, I) monolayers are 2D FM BMS with dynamic stability, thermal stability, and mechanical stability by first-principles calculations. The critical temperatures of both $PdCl_2$ and $PdBr_2$ monolayers are higher than the boiling point of liquid nitrogen (77 K). Moreover, the BMS characteristics of $PdCl_2$ and $PdBr_2$ are robust against external strains and strong electric fields, which is conducive to their applications. The carrier doping can induce the change between the semiconductor and half metal. Furthermore, we manipulate the spin polarization of $PdCl_2$ and $PdBr_2$ by introducing the FE gate to enable magnetic half-metal/semiconductor switching and spin-up/down polarization switching control. Finally, based on this, we realize two kinds of spin devices (multiferroic memory and spin filter). As well as proposing two novel BMS materials: $PdCl_2$ and $PdBr_2$, this study provides a theoretical basis for the development of spin devices.

Acknowledgments

Project supported by the Taishan Scholar Program of Shandong Province, China (Grant No. ts20190939), the Independent Cultivation Program of Innovation Team of Jinan City (Grant No. 2021GXRC043), the National Natural Science Foundation of China (Grant No. 52173283), and the Natural Science Foundation of Shandong Province (Grant No. ZR2020QA052).

References

[1] Cui Q, Liang J, Shao Z, Cui P and Yang H 2020 *Phys. Rev. B* **102** 094425
[2] Cui Q, Zhu Y, Liang J, Cui P and Yang H 2021 *Phys. Rev. B* **103** 085421
[3] Chen J, Guo Y, Ma C, Gong S, Zhao C, Wang T, Dong X, Jiao Z, Ma S, Xu G and An Y 2023 *Phys. Rev. Appl.* **19** 054013
[4] Wang Y P, Ji W X, Zhang C W, Li P, Zhang S F, Wang P J, Li S S and Yan S S 2017 *Appl. Phys. Lett.* **110** 213101
[5] Jia K, Dong X J, Li S S, Ji W X and Zhang C W 2023 *Nanoscale* **15** 8395
[6] Sun H, Li S S, Ji W X and Zhang C W 2022 *Phys. Rev. B* **105** 195112
[7] Zhang M H, Zhang C W, Wang P J and Li S S 2018 *Nanoscale* **10** 20226
[8] Zhang S J, Zhang C W, Zhang S F, Ji W X, Li P, Wang P J, Li S S and Yan S S 2017 *Phys. Rev. B* **96** 205433
[9] De Groot R A, Mueller F M, Van Engen P G and Buschow K H J 1983 *Phys. Rev. Lett.* **50** 2024
[10] Kan E, Li Z, Yang J and Hou J G 2008 *J. Am. Chem. Soc.* **130** 4224
[11] Son Y W, Cohen M L and Louie S G 2007 *Nature.* **446** 342
[12] Du A, Sanvito S and Smith S C 2021 *Phys. Rev. Lett.* **108** 197207
[13] Wang L, Cai Z, Wang J, Lu J, Luo G, Lai L, Zhou J, Qin R, Gao Z, Yu D, Li G, Mei W N and Sanvito S 2008 *Nano Lett.* **8** 3640
[14] Wu B, Song Y L, Ji W X, Wang P J, Zhang S F and Zhang C W 2023 *Phys. Rev. B* **107** 214419
[15] Kan E, Hu W, Xiao C, Lu R, Deng K, Yang J and Su H 2012 *J. Am. Chem. Soc.* **134** 5718
[16] Zhou J and Sun Q 2011 *J. Am. Chem. Soc.* **133** 15113
[17] Zhang M H, Zhang S F, Wang P J and Zhang C W 2020 *Nanoscale* **12** 3950
[18] Yue Z, Li Z, Sang L and Wang X 2020 *Small* **16** 1905155
[19] Li X, Wu X, Li Z, Yang J and Hou J G 2012 *Nanoscale* **4** 5680
[20] Li X and Yang J 2013 *Phys. Chem. Chem. Phys.* **15** 15793
[21] Li J, Li X and Yang J 2022 *Fundamental Research* **2** 511
[22] Zhao Y, Zhang J, Yuan S and Chen Z 2019 *Adv. Funct. Mater.* **29** 1901420
[23] Sun Y, Zhuo Z and Wu X 2018 *J. Mater. Chem. C* **6** 11401
[24] Han Y T, Ji W X, Wang P J, Li Ping and Zhang C W 2023 *Nanoscale* **15** 6830
[25] Zhang J, Zhao B, Ma C and Yang Z 2021 *Phys. Rev. B* **103** 075433
[26] Aminzadeh H and Nasresfahani Sh 2022 *Appl. Surf. Sci.* **581** 152338
[27] Wu Z, Cheng X and Zhang H 2023 *J. Magn. Magn. Mater.* **566** 170310
[28] Abdurakhmanova N, Tseng T C, Langner A, Kley C S, Sessi V, Stepanow S and Kern K 2013 *Phys. Rev. Lett.* **110** 027202
[29] Baibich M N, Broto J M, Fert A, Van Dau F N, Petroff F, Etienne P, Creuzet G, Friederich A and Chazelas J 1988 *Phys. Rev. Lett.* **61** 2472
[30] Li Y, Deng J, Zhang Y F, Jin X, Dong W H, Sun J T, Pan J and Du S 2023 *NPJ Comput. Mater.* **9** 50
[31] Kresse G and Joubert D 1999 *Phys. Rev. B* **59** 1758
[32] Kresse G and Furthmüller J 1996 *Phys. Rev. B* **54** 11169
[33] Kresse G and Hafner J 1994 *Phys. Rev. B* **49** 14251
[34] Perdew J P, Burke K and Ernzerhof M 1996 *Phys. Rev. Lett.* **77** 3865
[35] Calderon C E, Plata J J, Toher C, Oses C, Levy O, Fornari M, Natan A, Mehl M J, Hart G, Buongiorno Nardelli M and Curtarolo S 2015 *Comput. Mater. Sci.* **108** 233
[36] Dudarev S L, Botton G A, Savrasov S Y, Humphreys C J and Sutton A P 1998 *Phys. Rev. B* **57** 1505
[37] Togo A, Oba F and Tanaka I 2008 *Phys. Rev. B* **78** 134106
[38] Kresse G and Hafner J 1993 *Phys. Rev. B* **47** 558
[39] Grimme S 2006 *J. Comput. Chem.* **27** 1787
[40] Bučko T, Hafner J, Lebègue S and Ángyán J G 2010 *J. Phys. Chem. A* **114** 11814
[41] Wang V, Xu N, Liu J C, Tang G and Geng W T 2021 *Comput. Phys. Commun.* **267** 108033
[42] Liu L, Ren X, Xie J, Cheng B, Liu W, An T, Qin H and Hu J 2019 *Appl. Surf. Sci.* **480** 300
[43] Bolen E, Deligoz E and Ozisik H 2021 *Solid. State. Commun* **327** 114223
[44] Hoat D M, Vu T V, Obeid M M and Jappor H R 2019 *Superlattices Microstruct.* **130** 354
[45] Naseri M, Hoat D M, Salehi K and Amirian S 2020 *J. Mol. Graph. Model* **95** 107501
[46] Zhang Y, Hou B, Wu Y, Chen Y, Xia Y, Mei H, Kong M, Peng L, Shao H, Cao J, Liu W, Zhu H and Zhang H 2022 *Mater. Today Phys.* **22** 100604
[47] Ran R, Cheng C, Zeng Z Y, Chen X R and Chen Q F 2019 *Philosophical Magazine* **99** 1277
[48] Peng B, Mei H, Zhang H, Shao H, Xu K, Ni G, Jin Q, Soukoulis C M and Zhu H 2019 *Inorg. Chem. Front.* **6** 920

[49] Zhidkov I S, Akbulatov A F, Poteryaev A I, Kukharenko A I, Rasmetyeva A V, Frolova L A, Troshin P A and Kurmaev E Z 2023 *Coatings* **13** 784
[50] Lu F, Wang W, Luo X, Xie X, Cheng Y, Dong H, Liu H and Wang W H 2016 *Appl. Phys. Lett.* **108** 132104
[51] Meng R and Houssa M 2023 *Sci. Rep.* **13** 11521
[52] Yagmurcukardes M, Peeters F M and Sahin H 2018 *Phys. Rev. B* **98** 85431
[53] Parlinski K, Li Z Q and Kawazoe Y 1997 *Phys. Rev. Lett.* **78** 4063
[54] Blonsky M N, Zhuang H L, Singh A K and Hennig R G 2015 *ACS Nano* **9** 9885
[55] Andrew R C, Mapasha R E, Ukpong A M and Chetty N 2012 *Phys. Rev. B* **85** 125428
[56] Weiss A 1964 *Ber. Bunsenges. Phys. Chem.* **68** 996
[57] Becke A D and Edgecombe K E 1990 *J. Chem. Phys.* **92** 5397
[58] Savin A, Jepsen O, Flad J, Andersen O K, Preuss H and Von Schnering H G 1992 *Angew. Chem. Int. Ed.* **31** 187
[59] Savin A, Nesper R, Wengert S and Fässler T F 1997 *Angew. Chem. Int. Ed.* **36** 1808
[60] Hernández-Trujillo J and Bader R F W 2000 *J. Phys. Chem. A* **104** 1779
[61] Deng J, Guo J, Hosono H, Ying T and Chen X 2021 *Phys. Rev. Mater.* **5** 034005
[62] Kosterlitz J M and Thouless D J 1973 *J. Phys. C: Solid State Phys.* **6** 1181
[63] Ding W, Zhu J, Wang Z, Gao Y, Xiao D, Gu Y, Zhang Z and Zhu W 2017 *Nat. Commun.* **8** 14956
[64] Soleimani M and Pourfath M 2020 *Nanoscale* **12** 22688